Proceedings of IDETC/CIE 2008
ASME 2008 International Design Engineering Technical Conferences &
Computers and Information in Engineering Conference
August 3-6, 2008, Brooklyn, New York, USA

DETC2008-50072

OPTIMIZATION OF A PLANAR QUADRUPED DYNAMIC LEAP

Subhrajit Bhattacharya*
Department of Mechanical Engineering and
Applied Mechanics
University of Pennsylvania
Philadelphia, PA 19104
Email: subhrabh@seas.upenn.edu

Sachin Chitta
Department of Mechanical Engineering and
Applied Mechanics
University of Pennsylvania
Philadelphia, PA 19104
Email: sachinc@seas.upenn.edu

Vijay Kumar
Department of Mechanical Engineering and
Applied Mechanics
University of Pennsylvania
Philadelphia, PA 19104
Email: kumar@me.upenn.edu

Daniel Lee
Department of Electrical and
Systems Engineering
University of Pennsylvania
Philadelphia, PA 19104
Email: ddlee@seas.upenn.edu

ABSTRACT

Quadruped walking robots need to handle high obstacles like steps that are often not kinematically reachable. We present a dynamic leap that allows a quadruped robot to put its front legs up onto a high rock or ledge, a motion we have found is critical to being able to locomote over rough terrain. The leaping motion was optimized using a simulated planar quadruped model. We present experimental results for the implementation of this optimized motion on a real quadruped robot.

1 Introduction

Quadruped robots must be capable of locomoting over a wide variety of terrain including high steps and ledges. Such obstacles present a significant challenge since they are often kinematically difficult for the robot to overcome. Step climbing is in particular an important skill for walking robots in urban environments. Current approaches to step-climbing for walking robots fall into two categories, statically stable or quasi-static gaits and dynamic gaits.

Dynamic gaits have been extensively used for obstacle and stair climbing in robots with compliant legs like the SCOUT [1, 2] and RHex robotic platforms [3]. These robots are capable of true *leaping behavior* since the compliance in the legs can be used to store energy for subsequent release to initiate leaping. However, for high steps, RHex reverts back to using a simpler non-dynamic gait that moves the robot slowly over the steps.

Design, mathematical modeling and control of running and galloping gaits for quadrupeds have been studied extensively in the past [4, 5, 6]. Similar investigations have been made for bipeds [7, 8]. However such gaits have been designed primarily for flat terrains or terrains with moderate undulations. A more aggressive dynamic behavior is needed in order to negotiate with terrain features like steps, barriers, or terrains with certain level of uncertainties.

There is a long history and extensive literature on quasi-static gaits for quadrupeds and hexapods demonstrating remarkable abilities to negotiate rough terrain using quasi-static gaits [9, 10, 11]. The gaits are *crawl* gaits where three or more

*Address all correspondence to this author

legs are in contact with the ground forming a stable polygon of support. The robots can negotiate obstacles on the scale of the robot itself. The requirement for the gaits to be quasi-statically stable, however, results in a slow and unreliable execution, especially for very high steps.

A quasi-static sequence is often used to climb onto a step. For obstacles that are almost as high as the robot itself, the placement of the front feet on the step in this manner involves putting one front foot up on the step followed by the other. Kinematic reachability constraints limit this motion significantly and the overall motion of the robot is slow and unreliable. Further, the intermediate position with one foot at the base of the step and the other on the top of the step is a very awkward position for the robot to be in and limits the range of motion of the body.

In this work, we focus on designing a *dynamic* leaping motion to get the front feet onto the top of the step. Our focus on this particular part of the problem (of climbing onto a high step) is motivated by the difficulty in executing this motion using quasi-static gaits for a quadruped. We use a simplified planar model of the quadruped to develop the leaping behavior. The leap is then optimized to be able to step up onto a very high step. We also present experimental results from the implementation of the leaping behavior on an experimental platform called LITTLEDOG. This platform is manufactured by BOSTON DYNAMICS and is described in Section 2.

The simplified planar model developed here for optimization of the leaping behavior is similar to that defined for underactuated robots like the Acrobot [12]. The Acrobot is a two-link robot with a single actuator. Swing-up control of the Acrobot is achieved by exploiting the coupling between the two links. Our system is similarly underactuated and the dynamic coupling between the various parts of the system helps in driving it in the desired manner.

This paper is organized as follows. In Section 2, we present details of the Littledog robot used as the experimental platform for our research. A simplified planar dynamic model for the robot is discussed in Section 3. The design of the leaping behavior is presented in Section 4. Section 5 discusses the optimization of the behavior. Results from the implementation of the behavior on the experimental platform are presented in Section 6.

2 Experimental platform

The quadruped robot used as an experimental platform for this work is called LITTLEDOG (Figure 1) manufactured by Boston Dynamics Inc. The robot has four legs with three joints in each leg and can be powered either by onboard batteries or an external power system. Communication is through a wireless 802.11b connection with a host computer. Onboard sensing includes a three-axis accelerometer, gyroscopes and three-axis force sensors at the bottom of the feet.

The three joints in each leg are shown in Figure 1. The first two joints form the hip of the leg and allow motion about the X and Y axis while the third joint represents the knee motion about the Y axis.

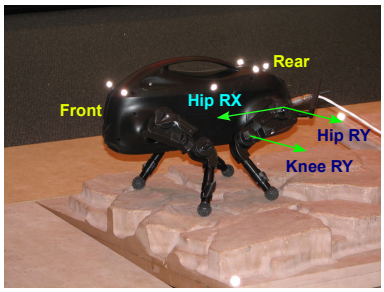

Figure 1. The LITTLEDOG robot

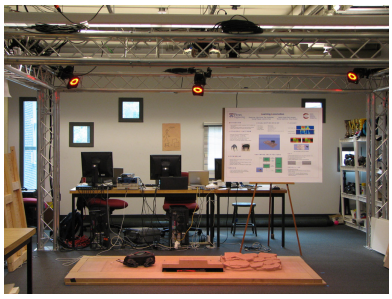

Figure 2. The VICON motion capture system used for ground truth.

The experimental setup includes a VICON motion capture system (Figure 2). This system consists of 6 high speed cameras operating at about 100 Hz. A set of reflective markers on the robot allows the system to track the position and orientation of the robot with sub-millimeter accuracy. We use this system for ground truth measurements to validate the experimental results against the simulated results.

3 Modeling and Simulation

3.1 Two dimensional abstraction

For developing a two-dimensional model of the LITTLEDOG robot we exploit the fact that the robot is symmetrical about the sagittal (XZ) plane. The two-dimensional abstraction is shown in Figure 3. Links 1 and 2 constitute the hind leg, and links 4 and 5 constitute the front leg. Link 3 represents the body of the robot. The lengths of these links are the same as those in the actual robot. Note that splitting the 3D robot by the vertical XZ plane results in splitting the body into two while the legs on each half stay the same. Hence, the legs of the 2D abstracted model have the same mass as the legs in the actual robot, but the mass of the body of the abstracted model is given by half the body mass of the actual robot. The mass of the body of LITTLEDOG is 2.240 Kg, and so $m_3 = 1.120$ Kg (see Appendix).

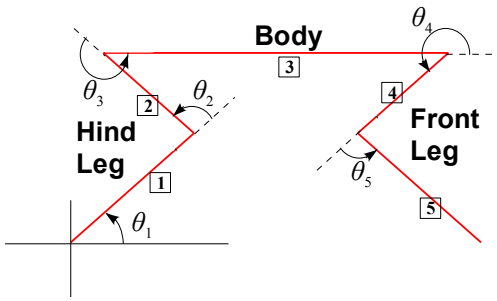

Figure 3. The 2D model of the Littledog robot

Figure 3 shows the 2 dimensional abstraction of the LITTLEDOG robot. The joints corresponding to $\theta_2, \theta_3, \theta_4$ and θ_5 are respectively the *hind knee*, *hind hip*, *front hip* and *front knee* joints. In our model, we assume that the hind foot is hinged to the ground at the heel (the origin in Figure 3). This is a realistic assumption for the particular problem under consideration, as described in Section 4.1. The 2D abstracted model has one unactuated joint (Joint 1) and four actuated joints (Joints 2 to 5). As shown, the configuration of the robot can be represented by the 5 joint angles $\theta_1, \theta_2, \theta_3, \theta_4$ and θ_5.

3.2 Dynamic model

We assume that there is no frictional resistance in the individual joints. We assume that the hind foot can stay at the same point on the the ground (i.e. the point of the hinge). On the other hand, we assume that no horizontal frictional forces act on the front foot when it is on the ground. These assumptions will be partly justified by the choice of strategy used for performing the leap (discussed in Section 4.1).

The ground is situated at the $y = 0$ line and passes through the origin. We assume that initially the front legs of the robot are touching the ground. We identify two states of the robot: The state when the front foot is touching the ground, and the state when the front foot is above the ground. We represent these two states using the parameter κ, which can assume the values 0 or 1 depending on the state. Thus,

$$\kappa = \begin{cases} 1 \text{ , if the front foot is in contact with the ground} \\ 0 \text{ , if the front foot is above the ground} \end{cases}$$

The leaping motion involves the robot starting off from the state $\kappa = 1$, and once it leaves the ground (i.e. switches to the $\kappa = 0$ state) it does not come back to the state $\kappa = 1$. We are primarily interested in the flight phase of the leap. The switch from the $\kappa = 1$ state to the $\kappa = 0$ state happens when the reaction force at the front foot becomes zero.

3.3 Constraints

Let the position vector of the front foot (*i.e.,* the end effector of the link) be given by $\mathbf{p}$. Then we can write,

$$\mathbf{p} = \left(\sum_{i=1}^{5} l_i \cos\left(\sum_{j=1}^{i} \theta_j \right) \right) \mathbf{e_1} + \left(\sum_{i=1}^{5} l_i \sin\left(\sum_{j=1}^{i} \theta_j \right) \right) \mathbf{e_2} \qquad (1)$$

where l_i is the length of the i^{th} link (see Appendix for the numerical values of the lengths), and θ_i is the joint angle as shown in the figure (measured counter-clockwise). $\mathbf{e_1}$ and $\mathbf{e_2}$ are the unit vectors along the horizontal and vertical axes directions respectively. We define $\mathbf{F} = F_x \mathbf{e_1} + F_y \mathbf{e_2}$ to be the reaction forces acting at the front foot, $\mathbf{p}$.

Let $\mathbf{u_1}$ and $\mathbf{u_2}$ be the unit vectors along the direction of the ground and the normal to the ground at the point of contact of the front foot. Define the normal reaction at the front foot as $F_N = \mathbf{F} \cdot \mathbf{u_2}$. The tangential component, $\mathbf{F} \cdot \mathbf{u_1}$, is always zero since we assume the absence of frictional resistance at the point of contact of the front foot.

When the front foot is in contact with the ground in the state corresponding to $\kappa = 1$, it cannot penetrate the ground. Further, in the state corresponding to $\kappa = 0$, the normal reaction on the front foot is zero. These two constraints can be written as,

$$\begin{aligned} \dot{\mathbf{p}} \cdot \mathbf{u_2} &= 0 \text{ , when } \kappa = 1 \\ F_N &= 0 \text{ , when } \kappa = 0 \end{aligned} \qquad (2)$$

When $\kappa = 1$, the front foot touches the ground, but is allowed to slide along the ground without any frictional resistance. We assume that $\mathbf{u_2}$ is a constant vector when $\kappa = 1$, *i.e.*, the ground is plain around the initial position of contact of the front foot. Note that Equations (2) can be written as complementary constraints [13]. But for the purpose of this paper, this explicit enumeration of states ($\kappa = 0, 1$) will suffice.

3.4 Lagrangian

We now define the Lagrangian for the abstracted 2-D model. The position of the center of mass of the q^{th} link is given by,

$$\begin{aligned} \mathbf{c}_q = &\left(\sum_{i=1}^{q-1} l_i \cos\left(\sum_{j=1}^{i} \theta_j \right) + \frac{l_q}{2} \cos\left(\sum_{j=1}^{q} \theta_j \right) \right) \mathbf{e_1} \\ &+ \left(\sum_{i=1}^{q-1} l_i \sin\left(\sum_{j=1}^{i} \theta_j \right) + \frac{l_q}{2} \sin\left(\sum_{j=1}^{q} \theta_j \right) \right) \mathbf{e_2} \end{aligned} \qquad (3)$$

The kinetic energy of the system is given by,

$$K = \sum_{i=1}^{5} \frac{1}{2} m_i \dot{\mathbf{c}}_i \cdot \dot{\mathbf{c}}_i + \sum_{i=1}^{5} \frac{1}{2} I_i \left(\sum_{j=1}^{i} \dot{\theta}_i \right)^2 \qquad (4)$$

where m_i is the mass of the i^{th} link and I_i is its moment of inertia about the center of mass (see the appendix for the numerical values of the inertial properties), and the potential energy is given by:

$$V = -\sum_{i=1}^{5} m_i \mathbf{g} \cdot \mathbf{c}_i \tag{5}$$

where $\mathbf{g} = -g\mathbf{e_2}$ is the acceleration due to gravity. The Lagrangian of the system is,

$$L = K - V \tag{6}$$

3.5 Equations of motion

The 5 equations of motion ($i = 1,2,3,4,5$) are given by,

$$\begin{aligned} \frac{d}{dt}\left(\frac{\partial L}{\partial \dot{\theta}_i}\right) - \frac{\partial L}{\partial \theta_i} - \tau_i - F_N \frac{\partial \dot{\mathbf{p}}}{\partial \dot{\theta}_i} \cdot \mathbf{u_2} = 0 \quad &, \text{when } \kappa = 1 \\ \frac{d}{dt}\left(\frac{\partial L}{\partial \dot{\theta}_i}\right) - \frac{\partial L}{\partial \theta_i} - \tau_i = 0 \quad &, \text{when } \kappa = 0 \end{aligned} \tag{7}$$

Equations (2) and (7) can be combined to write the equations defining the motion of the system concisely (for $i = 1,2,3,4,5$) as follows,

$$\begin{aligned} (1-\kappa)F_N + \kappa \dot{\mathbf{p}} \cdot \mathbf{u_2} = 0 \\ \frac{d}{dt}\left(\frac{\partial L}{\partial \dot{\theta}_i}\right) - \frac{\partial L}{\partial \theta_i} - \tau_i - \kappa F_N \frac{\partial \dot{\mathbf{p}}}{\partial \dot{\theta}_i} \cdot \mathbf{u_2} = 0 \end{aligned} \tag{8}$$

3.6 Simulation

Equation (8) consists of a total of 6 equations. The unknowns include F_N and a combination of θ_i's and τ_i's depending on whether are we commanding the joint angles or joint torques. However, in simulation, we will be providing torque commands for all the joints. Hence the quantities that need to be solved using the equations (8) are $F_N, \theta_1, \theta_2, \theta_3, \theta_4$ and θ_5. The state variables are $[\theta_1, \theta_2, \theta_3, \theta_4, \theta_5 \dot{\theta}_1, \dot{\theta}_2, \dot{\theta}_3, \dot{\theta}_4, \dot{\theta}_5]$, and the system of differential-algebraic equations are integrated using an implicit integration scheme.

Note that $\mathbf{u_2}$ is present in the equations (8) only for $\kappa = 1$. For $\kappa = 1$ the value of $\mathbf{u_2}$ remains constant and is equal to the direction normal to the ground. In the simplest case, $\mathbf{u_2} = \mathbf{e_2}$ when the ground is parallel to the horizontal axis.

We start the simulation in the state corresponding to $\kappa = 1$ and a configuration where the front foot is touching the ground. We assume $\dot{\theta}_i = 0$ at $t = 0$. The simulation switches from $\kappa = 1$ to $\kappa = 0$ when $F_N \leq 0$ and remains in the state with $\kappa = 0$ after that.

4 Control for a dynamic leap

4.1 Approach

In the dynamic leap, our objective is to use the hind foot/heel as a pivot point to lift up the body and the front leg. We start by defining a favorable initial condition (Figure 4) in which most of the body weight is carried by the hind legs and the front legs carry very little load. A large torque is then applied on the hind hip while stretching out the hind knee and simultaneously lifting up the front feet to complete the leap. Once the front leg is above the ground it does not play a significant role in the leaping control, although the inertia forces corresponding to motion of the front leg do influence the trajectory. We pull the front leg in to avoid collision with any obstacle lying ahead over which we want the robot to leap. The hind hip is torque controlled to track a desired torque profile while the other joints are controlled to track desired joint trajectories.

The strategy for the leap and the initial condition thus chosen explain our assumption about the reaction forces at the front and hind feet. The initial configuration ensures that most of the robot's body weight is concentrated at its hind foot, and only a very little weight is placed at the front foot. The normal reaction at the front foot will be much less compared to that at the hind foot, and hence so will be the frictional force. Thus our assumption that the robot is pivoted at the hind foot is justified.

4.2 Controller specifications

Joint 1 is unactuated and hence $\tau_1(t) = 0$ for all t. The controller specified a desired torque profile $\tau_3(t)$ for joint 3.

The desired torque for joints 2, 4 and 5 are obtained through a Proportional and Derivative (PD) controller. Because the joint torques are limited, a simple saturation model is used to implement the PD controller in simulation. Thus, the PD control law for $i = 2,4,5$ is given by,

$$\tau_i = \max\left\{ \min\left\{ k_p(\theta_i^d - \theta_i) + k_d(\dot{\theta}_i^d - \dot{\theta}_i), \tau_{max} \right\}, \tau_{min} \right\} \tag{9}$$

where k_p and k_d are the proportional and differential gains respectively; τ_{min} and τ_{max} are the lower and upper limits of the torques that the motors can apply. In both experiments and simulations, we used $k_p = 6.0$ and $k_d = 0.3$. These values were chosen based on experiments. The PD controller used for simulation, however, is different from the actual controller on the robot (as explained in Section 6.4) whose details are proprietary and not known.

4.3 Initial conditions

The initial configuration (Figure 4) is given by $\theta = (1.39, 1.31, 3.67, 4.29, 1.05)$. It is easy to show that in this configuration the reaction force at the hind foot is about 10.40 N,

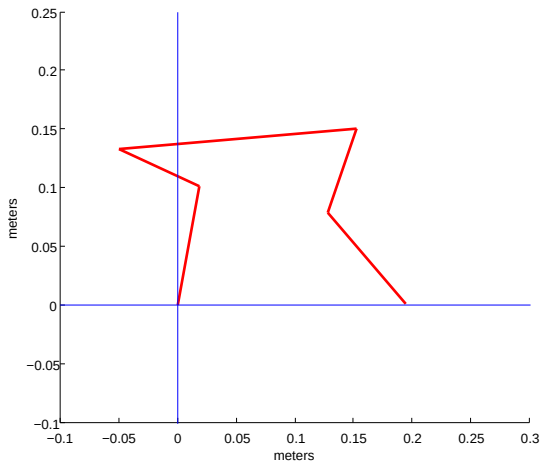

Figure 4. Initial configuration of the robot

whereas the reaction force at the front foot is about 4.32 N. A majority of the weight is thus carried by the hind foot in the initial configuration allowing the front foot to be easily lifted off the ground.

The initial joint velocities are chosen to be zero since the robot starts the leaping motion from rest in the initial configuration.

4.4 Torque and angle profiles

Figure 5 shows typical profiles used for τ_1, τ_3, θ_2^d, θ_4^d and θ_5^d. These are example profiles defined by several parameters that we will now discuss in detail. The optimization procedure outlined later will be used to optimize the leap over this set of parameters.

Although the plots in Figure 5 show the profiles for t from 0 to 0.7 seconds, experiments and simulations show that the leap occurs within the first 0.2 seconds. The remaining part of the profiles do not contribute significantly towards the procedure of leap. In subsequent plots, we will highlight the first 0.2 seconds of the motion. The desired profiles are specified by the following equations:

$$\begin{aligned}
\tau_1(t) &= 0 \\
\tau_3(t) &= f(t,\mu_{1,3},\mu_{2,3},\sigma_{1,3},\sigma_{2,3},H_{1,3},H_{2,3},h_{1,3},h_{2,3}) \\
\theta_2(t) &= f(t,\mu_{1,2},\mu_{2,2},\sigma_{1,2},\sigma_{2,2},H_{1,2},H_{2,2},h_{1,2},h_{2,2}) \\
\theta_4(t) &= f(t,\mu_{1,4},\mu_{2,4},\sigma_{1,4},\sigma_{2,4},H_{1,4},H_{2,4},h_{1,4},h_{2,4}) \\
\theta_5(t) &= f(t,\mu_{1,5},\mu_{2,5},\sigma_{1,5},\sigma_{2,5},H_{1,5},H_{2,5},h_{1,5},h_{2,5})
\end{aligned} \tag{10}$$

where f defines a 8-parameter family of *plateau-like* profiles. The key parameters used to describe f are the following:

$$f(t,\mu_1,\mu_2,\sigma_1,\sigma_2,H_1,H_2,h_1,h_2) = \begin{cases} h_1 + (H_1 - h_1)e^{-(\frac{t-\mu_1}{\sigma_1})^2} & , \text{if } t < \mu_1 \\ H_1 + \left(\frac{H_2 - H_1}{\mu_2 - \mu_1}\right) t & , \text{if } \mu_1 < t < \mu_2 \\ h_2 + (H_2 - h_2)e^{-(\frac{t-\mu_2}{\sigma_2})^2} & , \text{if } \mu_2 < t \end{cases}$$

The profile and the parameters are illustrated in Figure 5 (c). This class of desired profiles can approximate Gaussian and square impulses, step functions, smooth ramps and constant profiles reasonably well.

5 Optimization

The total number of parameters defining the initial configuration as well as the profiles for torque and desired angles is 36. The optimization procedure involves reducing the parameter space to a more manageable size and optimizing to find an optimum leaping behavior.

We used MATLAB's Optimization toolbox [14] to perform the optimization. Our optimization objective function is non-convex and non-smooth, but continuous in the parameters. The Optimization toolbox's *fmincon* is capable of handling such constrained nonlinear optimization problems, although it does not guarantee a global optimum. In practice, we found that solutions generated in this manner using the simulated model translated very well onto the actual robot.

5.1 Reducing the parameter set

To reduce the computational complexity of the problem, we chose to reduce the parameter set to a few critical parameters. The chosen parameters and their brief interpretations are listed below:

- $p_1 \equiv \mu_{1,3}$ → The time at which the peak torque value is reached at joint 3.
- $p_2 \equiv \sigma_{1,3}$ → The rise time to the peak torque from the initial value at joint 3.
- $p_3 \equiv H_{1,3}$ → The peak value of the torque reached at joint 3.
- $p_4 \equiv \mu_{1,4} = \mu_{1,5}$ → The time at which the front leg starts moving to pull itself back and subsequently stretch out.

5.2 Optimization objective

The obvious objective is to reach as high as possible with the front foot. Hence we would like to maximize the maximum height (h_{max}) attained by the leap. However, we would like to be able to negotiate *steep* obstacles, *i.e.* obstacles like steps that have a sharp rise in height over a very small horizontal distance.

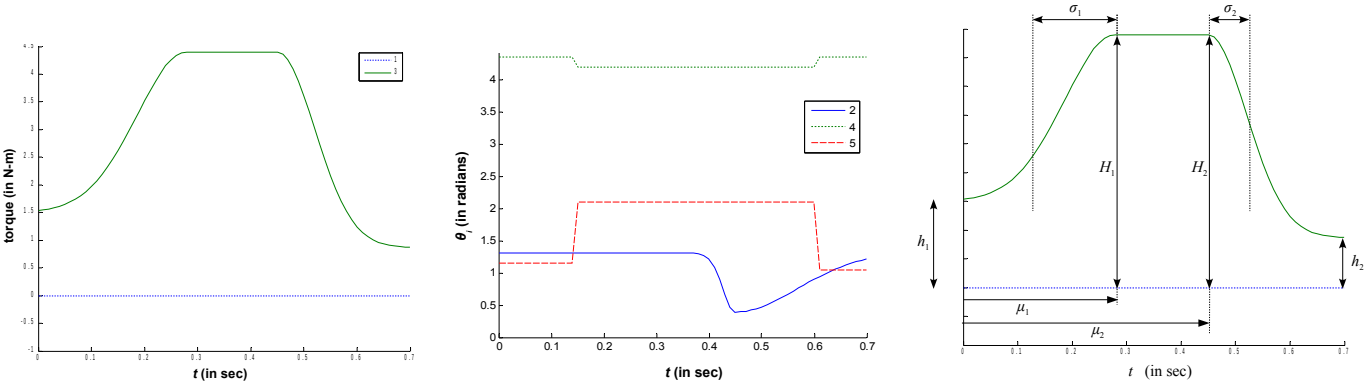

(a) Torque profiles (b) Joint angle profiles (c) The parametrized profile, f

Figure 5. Typical torque and joint angle profiles used in the simulations and experiments

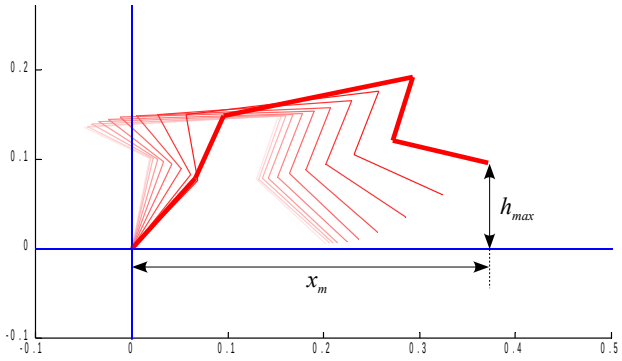

Figure 6. Objectives in a leap

Hence we also want to minimize the X-coordinate of the highest point in the climb (x_m). Another important criterion is to design trajectories that the onboard controller on the actual robot can track easily. Thus, we choose to maximize t_m, the time required to reach h_{max}. Slower motions are easier to implement by the onboard controllers without saturating the joint actuators.

We construct the optimization objective by combining these three distinct criteria. The optimization problem can be written as,

$$\min_{p_1,p_2,p_3,p_4} -\frac{h_{max}^2 t_m^{0.2}}{x_m}$$

The weights for h_{max} and t_m were chosen to give more importance to h_{max} and less importance to t_m.

6 Results

6.1 Case I: Unoptimized leap

An initial controller was first designed using a experimentally tuned set of values for the parameters for the desired torque and joint profiles. We used the following numerical values of the parameters to run the simulation as well as the experiment:

$$\begin{aligned}
&\mu_{1,3} = 0.28, \mu_{2,3} = 0.45, \sigma_{1,3} = 0.40, \sigma_{2,3} = 0.30,\\
&H_{1,3} = 3.40, H_{2,3} = 3.40, h_{1,3} = 0.50, h_{2,3} = -0.13;\\
&\mu_{1,2} = 0.45, \mu_{2,2} = 0.45, \sigma_{1,2} = 0.10, \sigma_{2,2} = 0.50,\\
&H_{1,2} = 0.39, H_{2,2} = 0.39, h_{1,2} = 1.31, h_{2,2} = 1.31;\\
&\mu_{1,4} = 0.15, \mu_{2,4} = 0.60, \sigma_{1,4} = 0.01, \sigma_{2,4} = 0.01,\\
&H_{1,4} = 4.19, H_{2,4} = 4.19, h_{1,4} = 4.29, h_{2,4} = 4.29;\\
&\mu_{1,5} = 0.15, \mu_{2,5} = 0.60, \sigma_{1,5} = 0.01, \sigma_{2,5} = 0.01,\\
&H_{1,5} = 2.09, H_{2,5} = 2.09, h_{1,5} = 1.15, h_{2,5} = 1.05;
\end{aligned}$$

The initial configuration was given by $\theta = (1.39, 1.31, 3.67, 4.29, 1.05)$, $\dot{\theta} = (0,0,0,0,0)$. The results obtained using these parameter values are summarized in Figure 7 and by the simulation snapshots shown in Figure 8.

6.2 Case II: Optimized leap

We performed the optimization procedure over the following bounded set of parameters:

$$\begin{aligned}
p_1 &\equiv \mu_{1,3} &&\in [0.05, 0.40]\\
p_2 &\equiv \sigma_{1,3} &&\in [0.05, 1.00]\\
p_3 &\equiv H_{1,3} &&\in [1.00, 3.40]\\
p_4 &\equiv \mu_{1,4} = \mu_{1,5} &&\in [0.05, 0.20]
\end{aligned}$$

It can be noted that in the particular case of p_3, the choice of the upper limit of 3.4 was motivated by the fact that the maximum allowable torque for the joint is about 3.4 N-m. The rest of the

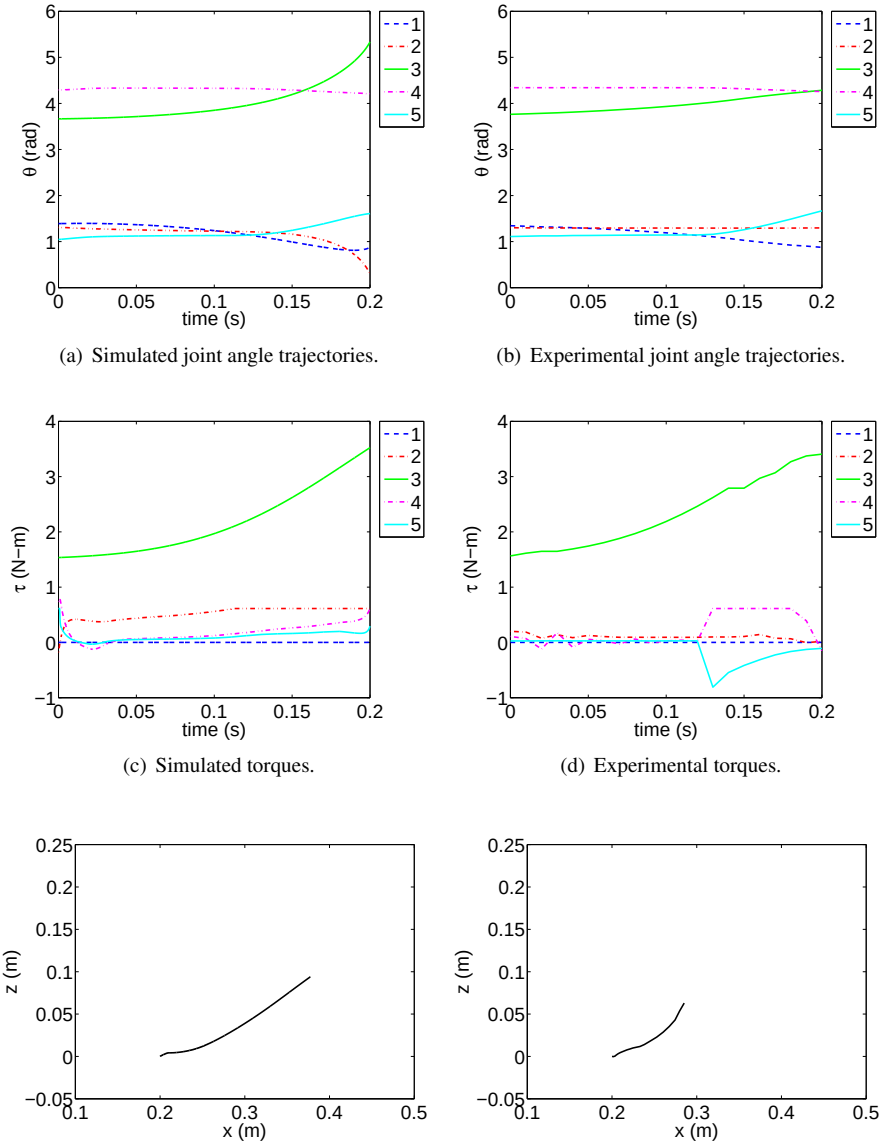

(a) Simulated joint angle trajectories.

(b) Experimental joint angle trajectories.

(c) Simulated torques.

(d) Experimental torques.

(e) Trajectory of front foot in simulation.

(f) Trajectory of front foot in experiment.

Figure 7. With unoptimized parameters: Comparison of simulated and experimental torque profiles, angle profiles and front foot trajectory

ranges were chosen around the values that were used for the *unoptimized leap*. The values for all the other parameters were the same as those used in the *unoptimized leap*.

The optimization procedure returned the following optimized values for the parameters: $\mu_{1,3} = 0.3790, \sigma_{1,3} = 0.6853$, $H_{1,3} = 3.4000, \mu_{1,4} = \mu_{1,5} = 0.0564$

The plots in Figure 9, the experimental snapshots in Figure 11 and the simulation snapshots in Figure 10 summarize the results obtained with these optimized parameters. A video demonstrating the leap to climb a short step can be found at [15].

6.3 Discussion

The success of optimizing over the chosen set of parameters becomes quite evident by comparing the plots in Figure 7 with those in Figure 9. However for better clarity and comparison we present the plots in Figure 12 comparing the unoptimized and optimized trajectories of the front foot. The height and the range achieved by the front foot is larger with optimized parameters than with the unoptimized parameters (for both experiments and simulation).

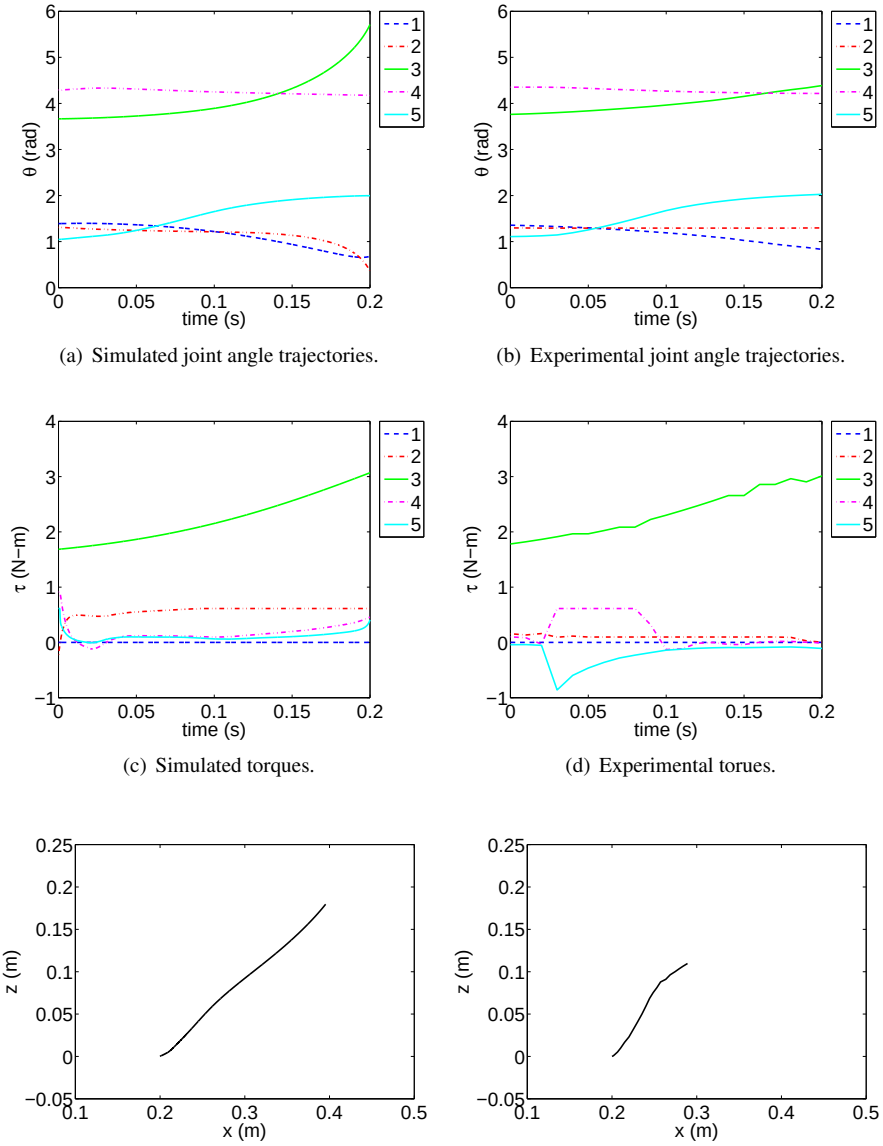

(a) Simulated joint angle trajectories.

(b) Experimental joint angle trajectories.

(c) Simulated torques.

(d) Experimental torues.

(e) Trajectory of front foot in simulation.

(f) Trajectory of front foot in experiment.

Figure 9. With optimized parameters: Comparison of simulated and experimental torque profiles, angle profiles and front foot trajectory

6.4 Comparison of simulated and experimental results

As noted earlier, the simulated model is an approximation. The simulation does not take into consideration any frictional resistance because of friction in the joints. Further, it does not incorporate a dynamic model for the actuators.

The contact between the foot and the ground is hard to simulate. We assumed that there is sufficient friction between the hind foot and the ground so as to keep the robot pivoted at the hind foot. We also assumed absence of any frictional force at the contact of the front foot and the ground. This hypothesis was inspired by the fact that in the initial configuration most of the robot's body weight is concentrated at its hind foot, and only a very little weight is placed at the front foot. Thus the normal reaction and hence the friction force at the front foot will be much less compared to those at the hind foot. In the robot these assumptions are valid only partially, and there may be some slippage at the hind feet and frictional force at the front feet.

There is a difference between the implementation of the PD controllers in simulation and the implementation on the robot.

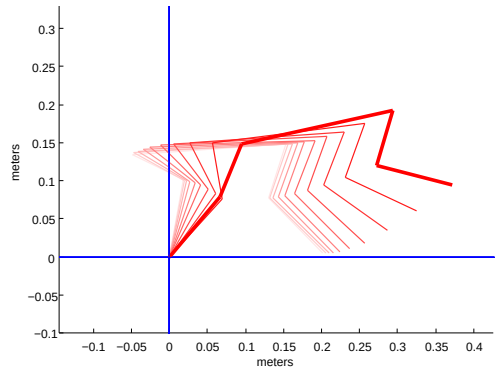

Figure 8. Snapshots from the simulation showing the leap performed with unoptimized parameters

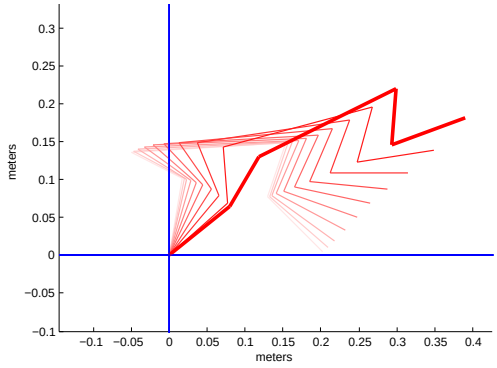

Figure 10. Snapshots from the simulation showing the leap performed with optimized parameters

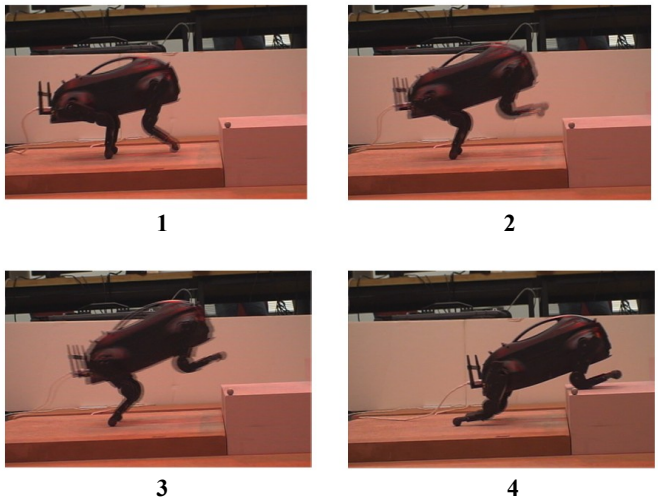

Figure 11. Snapshots from the actual experiment performed on the LITTLEDOG robot with optimized parameters

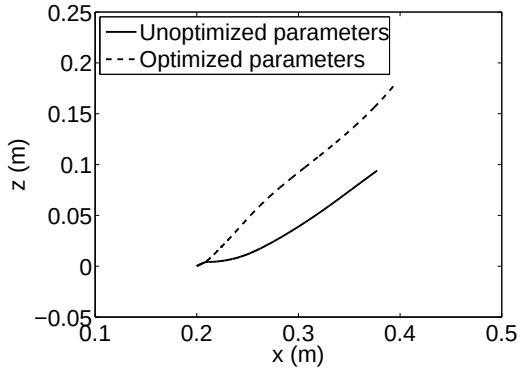

(a) Trajectory of front foot in simulation.

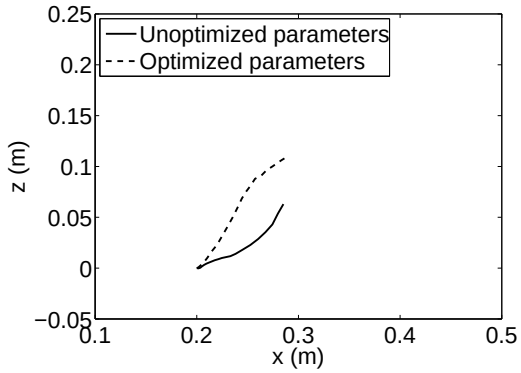

(b) Trajectory of front foot in experiment.

Figure 12. Simulated and experimental trajectories with unoptimized and optimized parameters

This explains the differences between the torque profiles in simulation and experiments for joints 2, 4 and 5. The commanded torque profiles for joint 3 were the same for both simulation and experiment, but the actual profiles were slightly different. This could be due to noise in the controller that controls the torque going to the motor.

In spite of the differences, the simulation model and optimization method has proved to be quite effective in finding a good set of parameters for the leap.

6.5 Complete Gait

To complete the motion of climbing onto the step, the hind legs are brought up onto the step using a quasi-static gait. Starting from the initial position with the front legs on the top of the step, the robot moves forward on its front knees until the hind legs are closer to the step. The robot then folds the hind legs up and places the hind feet onto the step and then moves forward using a *crawling* gait to get onto the step completely.

7 Conclusion

We have presented an approach to designing a *dynamic leap* for a quadruped robot. The leap was designed for the LITTLEDOG quadruped robot which has limited dynamic capabilities. Using a combination of this leap and a quasi-static gait, the robot is able to climb up onto a high step. The leap was optimized by choosing a particular parameterization of the inputs. The optimization resulted in the ability to leap higher and farther. The use of a simplified model was of significant help in developing the optimized gait. Although this gait was developed for a particular robot, the general approach can be extended to other walking robots.

The dynamic leap forms an important part of our strategy to be able to negotiate rough terrain at high speeds. We have found that getting up onto the terrain plays an important role in being successful in this task, especially when the obstacles are steep (like high steps). Other approaches to designing dynamic gaits for LITTLEDOG include the use of learning techniques. We are currently exploring the use of such techniques to develop better gaits to negotiate rough terrain.

8 Appendix

Dimensions and masses of the links of the two dimensional abstraction of the LITTLEDOG robot:

Link, i	Mass, m_i (in Kgs)	Length, l_i (in m)
1	0.095	0.1027
2	0.095	0.0751
3	1.120	0.2030
4	0.095	0.0751
5	0.095	0.1027

Moment of inertia of links 1, 2, 4 and 5 (about their center of masses) are computed as $I_i = \frac{1}{12} m_i l_i^2$, $i = 1,2,4,5$. Moment of inertia of link 3, the body, (about its center of mass) is computed as $I_3 = \frac{1}{12} m_i (l_i^2 + h^2)$, where $h = 0.143$ is the height of the body.

9 Acknowledgements

We gratefully acknowledge the support of ARO Grant W911NF-04-1-0148, NSF Grant IIS-0413138, ONR Grant N00014-07-1-0829, and DARPA Grant FA8650-05-C-7260. The second author would like to acknowledge Willow Garage, Inc. for their support.

REFERENCES

[1] Buehler, M., Battaglia, R., Cocosco, A., Hawker, G., Sarkis, J., and Yamazaki, K., 1998. "SCOUT: A simple quadruped that walks, climbs, and runs.". In IEEE International Conference on Robotics and Automation, pp. 1701–1712.

[2] Talebi, S., Buehler, M., and Papadopoulos, E., 2000. "Towards dynamic step climbing for a quadruped robot with compliant legs". In 3rd. International Conference on Climbing and Walking Robots.

[3] Moore, E. Z., Campbell, D., Grimminger, F., and Buehler, M., 2002. "Reliable stair climbing in simple Hexapod RHEX". In IEEE International Conference on Robotics and Automation, pp. 2222–2227.

[4] Schmiedeler, J. P., and Waldron, K. J., 1999. "The mechanics of quadrupedal galloping and the future of legged vehicles". *International Journal of Robotics Research,* **18**(12), pp. 1224–1234.

[5] ZOU, H., and Schmiedeler, J. P., 2004. "Dynamic modeling of quadrupedal running gaits using a simple template with asymmetrical body mass distribution". In Proceedings of the 2004 ASME International Design Engineering Technical Conferences.

[6] Schmiedeler, J. P., Waldron, K. J., Marhefka, D. W., and Orin, D. E., 1999. "Design of compliant articulated limbs for a quadrupedal galloping machine". In Proceedings of the Sixth Applied Mechanisms & Robotics Conference.

[7] Chevallereau, C., Westervelt, E. R., and Grizzle, J. W., 2004. "Asymptotic stabilization of a five-link, four-actuator, planar bipedal runner". In IEEE Conference on Decision and Control.

[8] Westervelt, E. R., Buche, G., and Grizzle, J. W., 2004. "Inducing dynamically stable walking in an underactuated prototype planar biped". In IEEE International Conference on Robotics and Automation.

[9] Stolle, M., and Atkeson, C., 2007. "Transfer of policies based on trajectory libraries". In Proceedings of the International Conference on Intelligent Robots and Systems (IROS 2007).

[10] Rebula, J. R., Neuhaus, P., Bonnlander, B. V., Johnson, M. J., and Pratt, J. E., 2007. "A controller for the littledog quadruped walking on rough terrain". In ICRA, pp. 1467–1473.

[11] Pongas, D., Mistry, M., and Schaal, S., 2007. "A robust quadruped walking gait for traversing rough terrain". In ICRA, pp. 1474–1479.

[12] Spong, M. W., 1995. "The swingup control problem for the Acrobot". *IEEE Control Systems Magazine,* **15**(1), February, pp. 49–55.

[13] Cottle, R. W., Pang, J. S., and Stone, R. E., 1992. *The Linear Complementary Problem*. Academic Press, Boston.

[14] MATLAB. *The* MATLAB *Optimization Toolbox*, 3.1.2 ed. The MathWorks. See also URL http://www.mathworks.com/products/optimization/.

[15] Bhattacharya, Chitta, Kumar, and Lee. Leap of the LITTLEDOG robot with optimized parameters. See URL http://www.seas.upenn.edu/ ∼subhrabh/ nonWebsite/ LittleDog/ DynamicLeap/dynamic_leap.html.